A functional Ni-Ni-[4Fe-4S] cluster in the monomeric acetyl-CoA synthase from *Carboxydothermus hydrogenoformans*

Vitali Svetlitchnyi*[†‡], Holger Dobbek[†§], Wolfram Meyer-Klaucke[¶], Thomas Meins*, Bärbel Thiele*, Piero Römer*, Robert Huber[‖], and Ortwin Meyer*[,]**

*Lehrstuhl für Mikrobiologie, [§]Lehrstuhl für Biochemie, and **Bayreuther Zentrum für Molekulare Biowissenschaften (BZMB), Universität Bayreuth, D-95440 Bayreuth, Germany; [¶]European Molecular Biology Laboratory, Outstation Hamburg at Deutsches Elektronen-Synchrotron, D-22603 Hamburg, Germany; and [‖]Abteilung Strukturforschung, Max-Planck-Institut für Biochemie, D-82152 Martinsried, Germany

Edited by Jack Halpern, University of Chicago, Chicago, IL, and approved November 14, 2003 (received for review July 9, 2003)

In anaerobic microorganisms employing the acetyl-CoA pathway, acetyl-CoA synthase (ACS) and CO dehydrogenase (CODH) form a complex (ACS/CODH) that catalyzes the synthesis of acetyl-CoA from CO, a methyl group, and CoA. Previously, a [4Fe-4S] cubane bridged to a copper-nickel binuclear site (active site cluster A of the ACS component) was identified in the ACS_{Mt}/$CODH_{Mt}$ from *Moorella thermoacetica* whereas another study revealed a nickel-nickel site in the open form of ACS_{Mt}, and a zink-nickel site in the closed form. The ACS_{Ch} of the hydrogenogenic bacterium *Carboxydothermus hydrogenoformans* was found to exist as an 82.2-kDa monomer as well as in a 1:1 molar complex with the 73.3-kDa $CODHIII_{Ch}$. Homogenous ACS_{Ch} and ACS_{Ch}/$CODHIII_{Ch}$ catalyzed the exchange between [1-^{14}C]acetyl-CoA and ^{12}CO with specific activities of 2.4 or 5.9 μmol of CO per min per mg, respectively, at 70°C and pH 6.0. They also catalyzed the synthesis of acetyl-CoA from CO, methylcobalamin, corrinoid iron-sulfur protein, and CoA with specific activities of 0.14 or 0.91 μmol of acetyl-CoA formed per min per mg, respectively, at 70°C and pH 7.3. The functional cluster A of ACS_{Ch} contains a Ni-Ni-[4Fe-4S] site, in which the positions proximal and distal to the cubane are occupied by Ni ions. This result is apparent from a positive correlation of the Ni contents and negative correlations of the Cu or Zn contents with the acetyl-CoA/CO exchange activities of different preparations of monomeric ACS_{Ch}, a 2.2-Å crystal structure of the dithionite-reduced monomer in an open conformation, and x-ray absorption spectroscopy.

Reactions involving the fixation of carbon monoxide (CO) into activated acetyl groups on surfaces containing the sulfides of nickel and iron have been implicated in models of the chemoautotrophic origin of life (1, 2). These models adopt sequences of the acetyl-CoA pathway (Wood/Ljungdahl pathway), which is operative in CO_2 fixation by autotrophic acetogens, sulfidogens, and methanogens, as well as in acetate utilization by methanogens (3–7). The synthesis of acetyl-CoA in the pathway involves the functions of a NiFeS acetyl-CoA synthase (ACS), a NiFeS CO dehydrogenase (CODH), and a cobalt-containing corrinoid iron-sulfur protein (CoFeSP). ACS and CODH form a tight complex in all microorganisms that have been previously examined in that respect (4–6). ACS catalyzes the synthesis of acetyl-CoA from a methyl group donated by CoFeSP, CO, and CoA (Eq. **1**) (5, 6). CODH catalyzes the reduction of CO_2 to CO, which reappears in the carboxyl group of the acetyl residue formed (Eq. **2**) (5, 6).

$$[CH_3—Co^{3+}FeSP]^{2+} + CO + CoASH \rightarrow CH_3—CO—SCoA + Co^{+}FeSP + H^{+} \quad [1]$$

$$CO_2 + 2\ \text{electrons} + 2\ H^{+} \rightarrow CO + H_2O \quad [2]$$

Carboxydothermus hydrogenoformans is a hydrogenogenic bacterium that utilizes CO as a sole source of carbon and energy under anaerobic chemolithoautotrophic conditions (8). The bacterium presumably employs the acetyl-CoA pathway for the assimilation of carbon (V.S., personal communication). The genomic sequence of *C. hydrogenoformans* contains an ≈10-kb region that assembles the predicted functions of the genes *cooSIII* ($CODHIII_{Ch}$, 73.3 kDa), *acs* (ACS, 82.2 kDa), *cfsA* and *cfsB* (the 48.8-kDa large and the 33.9-kDa small subunits of the heterodimeric CoFeSP), and *mtr* (a 29.3-kDa methyltransferase) (Fig. 1*A*). The deduced amino acid sequence of *acs* from *C. hydrogenoformans* shows 74% identity (86% similarity) to the complexed ACS_{Mt} from *Moorella thermoacetica* (9).

According to a recent model (9), the generation of energy and reducing equivalents in *C. hydrogenoformans* involves the activities of the monofunctional $CODHI_{Ch}$ and $CODHII_{Ch}$. A first crystal structure of a NiFeS-CODH, the $CODHII_{Ch}$, at 1.6 Å resolution in the dithionite-reduced state showed five metal clusters, of which clusters B, B′, and a subunit-bridging, surface-exposed cluster D are cubane-type [4Fe-4S] clusters (10). The active-site clusters C and C′ are asymmetric [Ni-4Fe-5S] clusters. Their integral Ni ion, which is the likely site of CO oxidation, is coordinated by four sulfur ligands with square planar geometry. The $CODH_{Rr}$ crystal structure from *Rhodospirillum rubrum* determined at 2.8-Å resolution shows a similar overall structure, except that cluster C is interpreted as a [Ni-3Fe-4S] cubane, to which a mononuclear Fe site is coordinated (11). Cluster C in the CODH component of the ACS_{Mt}/$CODH_{Mt}$ complex from *M. thermoacetica* has been described as a Ni-4Fe-4S cage that can be viewed as a [Ni-Fe] subsite linked by three μ^3-bridging sulfide ions emanating from one face of a [3Fe-4S] subsite (12). The ACS_{Mt}/$CODH_{Mt}$ complex has previously been structurally characterized by using distinct crystal forms of the protein. The ACS_{Mt}/$CODH_{Mt}$ structures reported by Doukov *et al.* (13) and Darnault *et al.* (12) are generally similar and have an $\alpha_2\beta_2$ (α, ACS; β, CODH) quaternary structure. The structures of the $CODH_{Mt}$ subunits are similar in the two crystal forms and closely resemble the structures of $CODHII_{Ch}$ (10) and $CODH_{Rr}$ (11). The ACS_{Mt} component of the ACS_{Mt}/$CODH_{Mt}$ complex accommodates the active site cluster A, which is a [4Fe-4S] cubane bridged to a binuclear metal site. The metal site distal to the cubane contains a Ni ion (12, 13). The metal proximal to the cubane has been interpreted as Cu (13), as Zn (closed from of the ACS), or as Ni (open form of the ACS) (12), yielding Cu-Ni, Zn-Ni, and Ni-Ni binuclear sites. The Ni in cluster A is known to be labile and can be removed by 1,10-phenanthroline (14). A promiscuous proximal

This paper was submitted directly (Track II) to the PNAS office.

Abbreviations: ACS, acetyl-CoA synthase; CODH, CO dehydrogenase; CoFeSP, corrinoid iron-sulfur protein; XAS, x-ray absorption spectroscopy; EXAFS, x-ray absorption fine structure.

Data deposition: The atomic coordinates and structure factors have been deposited in the Protein Data Bank, www.rcsb.org (PDB ID code 1RU3).

[†]V.S. and H.D. contributed equally to this work.

[‡]To whom correspondence should be addressed. E-mail: vitali.svetlitchnyi@uni-bayreuth.de.

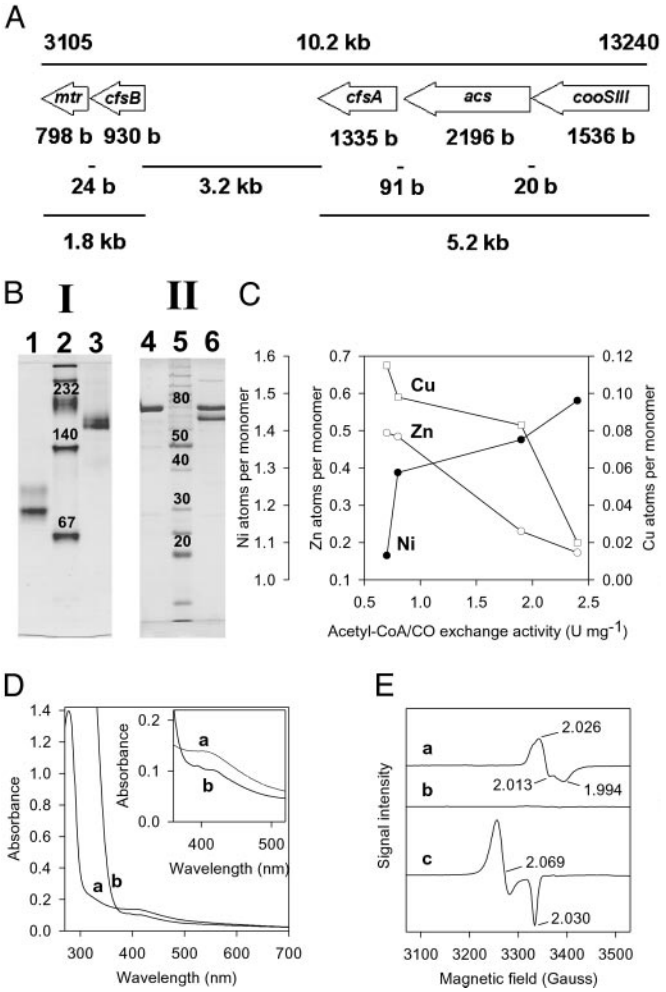

Fig. 1. (*A*) Organization of the ACS gene cluster in *C. hydrogenoformans*. The cluster contains the genes encoding the methyltransferase (*mtr*), the small (*cfsB*) and the large (*cfsA*) subunits of the CoFeSP, the ACS_{Ch} (*acs*), and the $CODHIII_{Ch}$ (*cooSIII*). (*B*) Analysis of ACS_{Ch} and $ACS_{Ch}/CODHIII_{Ch}$ by PAGE. The proteins were subjected to native PAGE (*I*) and SDS/PAGE (*II*). (*I*) Native PAGE: lane 1, 7.5 μg of ACS_{Ch}; lane 2, molecular mass markers (kDa); lane 3, 7.5 μg of $ACS_{Ch}/CODHIII_{Ch}$. (*II*) SDS/PAGE: lane 4, 10 μg of ACS_{Ch}; lane 5, molecular mass markers (kDa); lane 6, 10 μg of $ACS_{Ch}/CODHIII_{Ch}$. (*C*) Dependence of acetyl-CoA/CO exchange activity of the monomeric ACS_{Ch} on metal content. The data for activities and contents of Ni (filled circles), Zn (open circles), and Cu (open squares) for four different ACS_{Ch} preparations are from Table 1. (*D*) UV-visible absorption spectra of ACS_{Ch}. As-isolated oxidized ACS_{Ch} (11.3 μM, preparation 2 in Table 1) in 50 mM Tris·HCl, pH 8.0, under N_2 (trace a) was reduced with 4 mM dithionite for 10 min at 22°C (trace b). (*Inset*) Enlargement of the FeS-schoulder. (*E*) EPR spectra of ACS_{Ch}. As-isolated oxidized ACS_{Ch} (180 μM, preparation 2 in Table 1) in 50 mM Tris·HCl, pH 8.0, under N_2 (trace a) was treated with 4 mM dithionite for 10 min at 22°C (trace b) or kept under pure CO for 30 min at 22°C (trace c). The relevant *g* values are indicated in the spectrum. General conditions: 10-mW microwave power, 10-G modulation amplitude, 9.47-GHz microwave frequency, 20 K.

metal site in cluster A leaves the question of the true catalytic metal open. An essential and functional role of Cu in the ACS/CODH from acetogenic and methanogenic microorganisms was suggested from the correlation of Cu contents and acetyl-CoA/CO exchange activities in combination with spectroscopic measurements (15). On the other hand, data have been obtained consistent with a catalytically active Ni_2-cubane site. Ni restored the acetyl-CoA/CO exchange activities of $ACS_{Mt}/CODH_{Mt}$ deprived of the metal by treatment with 1,10-phenanthroline (16, 17) whereas Cu was inhibitory and not required for ACS activity (17). Ni also activated a recombinant apo ACS subunit from *Methanosarcina thermophila*, and other divalent metal ions could not substitute for Ni in yielding catalytic activity (18).

The genome of *C. hydrogenoformans* contains only a single copy of the *acs* gene, which is closely preceded by the *cooSIII* gene (Fig. 1*A*). We are showing in this paper that these genes produce in CO-grown cells a unique monomeric ACS_{Ch}, along with a complex of the ACS_{Ch} with a newly recognized $CODHIII_{Ch}$. The primary sequences of $CODHIII_{Ch}$ and the structurally characterized $CODHII_{Ch}$ are 47% identical and 67% similar to each other. ACS_{Ch} and $ACS_{Ch}/CODHIII_{Ch}$ were purified to homogeneity and shown to catalyze the acetyl-CoA/CO exchange reaction as well as the synthesis of acetyl-CoA from CoA, CO, and a methyl group.

We have studied the structure of the reduced monomeric ACS_{Ch} and its metal center (cluster A) by x-ray crystallography and identified by anomalous dispersion measurements at different wavelengths a Ni-Ni-[4Fe-4S] structure. X-ray absorption spectroscopy (XAS) confirmed the results. The acetyl-CoA/CO exchange activities of different preparations of monomeric ACS_{Ch} showed a positive correlation with the Ni contents and negative correlations with the Cu or Zn contents. Metal analyses of the $ACS_{Ch}/CODHIII_{Ch}$ complex revealed stoichiometric amounts of Ni and only trace amounts of Cu and Zn. The results are consistent with a catalytically active Ni-Ni-[4Fe-4S] cluster.

Materials and Methods

Organism and Cultivation. *C. hydrogenoformans* Z-2901 (DSM 6008) was grown as described (9) except that yeast extract was omitted from the medium. The CO supply rates during the cultivations were gradually increased from 0.02 to 0.5 liters of CO per min. Bacteria were harvested by centrifugation under N_2 at OD_{436} of ≈2.5, which corresponds to the end of the exponential growth phase, and kept frozen at −80°C under N_2.

Purification of Proteins. Purifications were carried out under anaerobic conditions as detailed (9). For cell lysis, ≈270 g of wet bacterial cell mass were suspended in 750 ml of 20 mM Tris·HCl (pH 7.4), supplemented with 5 mM dithionite, 0.1 mg·ml^{-1} lysozyme, 0.02 mg·ml^{-1} DNase I, and 0.2 mM PMSF, incubated for 30 min at 22°C with magnetic stirring, and subjected to low spin centrifugation. The resulting cell-free extracts were subjected to ultracentrifugation for 1 h at 160,000 × *g*. Cytoplasmic fractions (950 ml) were loaded onto anion exchange columns (25 × 5 cm, Source 30 Q, Amersham Pharmacia Biosciences) equilibrated with buffer A [20 mM Tris·HCl (pH 7.4), 3 mM dithionite]. Elution was with 1,500 ml of buffer A, followed by 1,500 ml of a linear 0 to 1 M gradient of NaCl in buffer A. The CoFeSP, ACS_{Ch}, and $ACS_{Ch}/CODHIII_{Ch}$ eluted at 0.4, 0.5, and 0.6 M NaCl, respectively. Fractions containing the corresponding proteins were pooled, supplemented with $(NH_4)_2SO_4$ to a final concentration of 1.5 M, and loaded onto hydrophobic interaction chromatography columns (12 × 5 cm, Source 15 ISO, Amersham Pharmacia Biosciences), equilibrated with 1.4 M $(NH_4)_2SO_4$ in buffer A. Elution was with 700 ml of equilibration buffer, followed by 1,360 ml of a linear decreasing 1.4 to 0 M gradient of $(NH_4)_2SO_4$ in buffer A. The CoFeSP, $ACS_{Ch}/CODHIII_{Ch}$, and ACS_{Ch} were recovered in the fractions eluting with 1.0, 0.8, and 0.7 M $(NH_4)_2SO_4$, respectively. Proteins were concentrated by ultrafiltration and subjected to gel filtration (columns 60 × 2.6 cm, Sephacryl S-200, Amersham Pharmacia Biosciences) employing buffer A supplemented with 150 mM NaCl. Purifications of ACS_{Ch} and $ACS_{Ch}/CODHIII_{Ch}$ were monitored by determination of the proteins by SDS/PAGE because first acetyl-CoA/CO exchange activities became detectable on hydrophobic interaction chromatography. The purified proteins were desalted by gel filtration on Sephadex G25 employing buffer A, concentrated by ultrafiltration, frozen in liquid N_2, and kept at −80°C.

The purified CoFeSP was identified on the basis of the molecular masses of its two subunits on SDS/PAGE (33 and 47 kDa) matching the masses of the predicted subunits (33.9 and 48.4 kDa), the N-terminal sequence of the small subunit (AVEVLKEKWN), and the presence of 0.8 mol of Co and 3.2 mol of Fe per mol of heterodimer.

Enzyme Assays. CO oxidation activity was assayed as described (9) by using methyl viologen as the electron acceptor. The [1-^{14}C]acetyl-CoA/CO exchange activity was assayed anaerobically in 17-ml tubes at 70°C following published procedures (19). The reaction mixtures (1 ml) contained 200 μM acetyl-CoA, 1.8 μM [1-^{14}C]acetyl-CoA (55 mCi/mmol)(1 Ci = 37 GBq), 3 mM Ti(III) citrate, and 1 mM DTT in 150 mM K-P_i buffer (pH 6.0) under pure CO. After initiation of the reactions through the addition of ACS_{Ch} or ACS_{Ch}/$CODHIII_{Ch}$, aliquots (100 μl) were taken from the reaction mixtures at regular intervals of 1.5 min and analyzed for radioactivity by liquid scintillation counting. Activities were calculated from the difference in the amount of radioactivity remaining in the aqueous phase as described (19) (an example of calculations can be found in *Supporting Materials and Methods*, which is published as supporting information on the PNAS web site). One unit of the exchange activity is defined as 1 μmol of CO exchanged per min.

Synthesis of acetyl-CoA was examined at 70°C by following acetyl-CoA formation from methylcobalamin, CO, and CoA, following published procedures (18, 20, 21). The assays were performed anaerobically in the dark in 2-ml vials. The reaction mixtures (0.5 ml) contained 1 mM methylcobalamin, 0.3 mg CoFeSP, 1 mM CoA, 1 mM Ti(III) citrate, and 1 mM DTT in 50 mM Hepes/NaOH (pH 7.3) under an atmosphere of 10% CO plus 90% N_2. Reactions were started by adding ACS_{Ch} or ACS_{Ch}/$CODHIII_{Ch}$. Aliquots were removed with time, immediately frozen in liquid N_2, and subsequently analyzed for the formation of acetyl-CoA by reversed phase (C18) HPLC employing 15% methanol in 100 mM K-Pi buffer (pH 5.5) as mobile phase.

Crystallization of ACS_{Ch}. Crystallization was performed in an anaerobic chamber filled with pure N_2 by using the hanging drop vapor diffusion method. Crystals of ACS_{Ch} were obtained at 17°C with $(NH_4)_2HPO_4$ as precipitant at a pH of 6.8 in the presence of 2 mM sodium-dithionite. Crystals usually appeared within 2 to 4 days. They were harvested after 10 days, shock frozen in reservoir solution supplemented with 25% (vol/vol) glycerol, and stored frozen in liquid N_2.

Structure Determination and Refinement. The enzyme crystallized in the rhombohedral space group H32 with cell parameters of $a = b = 200.5$ Å, $c = 169.9$ Å and one monomer per asymmetric unit. The position of the FeS cluster was determined after a multiwavelength anomalous diffraction (MAD) experiment at four different wavelengths at the Deutsches Elektronen-Synchrotron (DESY) synchrotron (BW6, Hamburg, Germany) by difference Patterson methods by using the program RSPS (22). Phases calculated with the program SHARP (23) and modified with SOLOMON (22) allowed the positioning of individual Fe atoms for the cubane-type [4Fe-4S] cluster of ACS_{Ch} by rigid body minimization of randomly orientated 4Fe-cubanes against Bijvoet-maps by using MAIN (24). The refined positions of 4 Fe atoms and 1 Ni atom were used as input positions for the experimental phasing (Table 3, which is published as supporting information on the PNAS web site). Subsequent solvent flattening using SOLOMON and DM (22) yielded interpretable electron density maps. After building the polypeptide chain, the additional metal sites of cluster A were located based on Bijvoet- and $2F_o - F_c$ maps. Several cycles of manual building with MAIN (24) and positional and temperature factor refinement with CNS (25) were carried out. Large parts of the middle domain (residues 316–500) showed an ill-defined electron density and have been modeled in similarity to the *M. thermoacetica* ACS_{Mt}/$CODH_{Mt}$ crystal structure (13). A dataset to 2.20-Å resolution was measured at the beamline ID14-EH2 (European Synchrotron Radiation Facility, Grenoble, France). The model was refined to 2.20-Å resolution with R_{cryst} of 0.237 and R_{free} of 0.274 and a good stereochemistry (Table 4, which is published as supporting information on the PNAS web site). The f″ values for Ni and Fe were refined by using CNS (25).

Ni-K Edge XAS. For XAS measurements, 45 μl of as-isolated ACS_{Ch} (oxidized state; 160 mg·ml^{-1}) were filled into sample cells of HESAR glass covered with Kapton windows. Cells were sealed and kept at temperatures below 194 K. XAS data were collected at the European Molecular Biology Laboratory beam line D2 (DESY, Hamburg, Germany) by using a Si (111) double monochromator and a focusing mirror. Absolute energy calibration of the spectra was achieved by Bragg reflections of a static Si (220) crystal in back reflection geometry (26). The sample was kept at ≈30 K in a two-stage Displex cryostat (modified Oxford Instruments, Oxon, U.K.). Spectra were recorded in fluorescence mode with a Canberra 13-element solid-state detector. The total Ni-Kα fluorescence count rate above 8,700 eV was >1,000,000 counts. Data reduction, such as background removal and extraction of the x-ray absorption fine structure (EXAFS), was achieved with the EXPROG program package (27), assuming E_0 of 8,333 eV for the photo-electron. EXAFS data (20–765 eV above E_0) were analyzed by using the refinement program EXCURV98 (28).

Miscellaneous Methods. Protein estimation used conventional methods (29, 30) with BSA as a standard. SDS/PAGE and native PAGE were performed as before (9). Protein transfer from polyacrylamide gels to poly(vinylidene difluoride) membranes and N-terminal amino acid sequencing followed published procedures (31). The molecular mass of proteins was determined by gel filtration on Superdex 200 columns (60 × 1.6 cm, Amersham Pharmacia Biosciences) equilibrated with buffer A. Metal contents were estimated by inductively coupled plasma atomic emission spectroscopy (ICP-AES, model Optima 3000, Perkin–Elmer) as well as by inductively coupled plasma mass spectroscopy (ICP-MS, model 7500 C, Agilent, Palo Alto, CA). Acid-labile sulfur was estimated colorimetrically (32). X-band EPR spectra were recorded on a Bruker EMX 6-1 spectrometer (Bruker, Rheinstetten, Germany) operated with a helium cryostat (Oxford Instruments) under the experimental conditions described (9).

Chemicals. All chemicals used were obtained from usual commercial sources. Gases were purchased from Riessner-Gase (Lichtenfels, Germany).

Results and Discussion

Purification of ACS_{Ch} and ACS_{Ch}/$CODHIII_{Ch}$. ACS_{Ch} was obtained from cytoplasmic fractions of *C. hydrogenoformans* grown under conditions of excess supply with CO. A typical purification procedure is documented in Table 5, which is published as supporting information on the PNAS web site. ACS_{Ch} was purified 42-fold to >93% of purity, with a yield of 12% and a specific exchange activity of 1.9 units·mg^{-1}. For the range of activities observed with different preparations, refer to Table 1. ACS_{Ch} is a significant constituent of the bacteria (≈2% of the total cell protein). The homogeneity of the ACS_{Ch} preparations obtained is apparent from a single 82.7-kDa band on native PAGE (Fig. 1*BI*, lane 1) and a single 82.9 kDa-band on SDS/PAGE (Fig. 1*BII*, lane 4). Gel filtration revealed a Stokes radius of 4.0 nm, corresponding to a molecular mass of 81.7 kDa. The experimentally determined molecular masses match the molecular mass of 82.2 kDa, which has been calculated from the deduced amino acid sequence of the *acs* gene. The results indicate that ACS_{Ch} is composed of a single polypeptide. The identity of the

Table 1. Acetyl-CoA/CO exchange activity and metal and acid-labile sulfur contents in ACS_{Ch} and $ACS_{Ch}/CODHIII_{Ch}$ from *C. hydrogenoformans* grown under different conditions of Cu supply

Enzyme species	Acetyl-CoA/CO exchange activity, units·mg^{-1}	$CuCl_2$*, μM	Metal and sulfur contents, moles/mole protein				
			Ni	Zn	Cu	Fe	S
ACS_{Ch}, per ACS_{Ch} monomer	2.4	0.4	1.48	0.17	0.02	3.54	4.18
	1.9	0.4	1.38	0.23	0.08	2.49	3.52
	0.8	4.0	1.29	0.48	0.10	3.49	2.79
	0.7	4.0	1.07	0.49	0.12	3.03	2.72
$ACS_{Ch}/CODHIII_{Ch}$, per $ACS_{Ch}/CODHIII_{Ch}$ heterodimer	5.9	0.4	2.47	0.05	0.04	11.56	11.34
	5.3	4.0	1.85	0.04	0.04	10.08	9.89
	3.6	4.0	2.50	0.06	0.06	11.68	10.65

*Indicated are the concentrations of $CuCl_2$ in the growth medium specified under *Materials and Methods.* The Ni contents were 50 μM $NiCl_2$.

purified ACS_{Ch} and the predicted product of the *acs* gene was apparent from the same N-terminal amino acid sequences (SEVINFDQIF).

$ACS_{Ch}/CODHIII_{Ch}$ was obtained from cytoplasmic fractions of *C. hydrogenoformans* grown under conditions of CO limitation. Employing the scheme of Table 5, $ACS_{Ch}/CODHIII_{Ch}$ was purified 29-fold to >95% of purity, with a yield of 13% and the specific exchange activities given in Table 1. The protein comprises 2.7% of the total cell protein. The single 185-kDa band on native PAGE (Fig. 1*BI*, lane 3) and the results of gel filtration, which indicated a Stokes radius of 6.6 nm, corresponding to a molecular mass of 385.82 kDa, were not consistent. The 82.9-kDa band (α) and the 70.1-kDa band (β) appearing on SDS/PAGE (Fig. 1*BII*, lane 6) which are present in a molar ratio of 1.17 $\pm$ 0.06:1 indicate the presence of two different polypeptides in $ACS_{Ch}/CODHIII_{Ch}$. The molecular masses and N termini of the α-subunit (SEVINFDQIF) and of the β-subunit (PRFRDLEHTS) match the molecular masses (82.2 kDa and 73.3 kDa) and the N termini of the predicted products of *acs* and *coosIII* (Fig. 1*A*).

The ratio between ACS_{Ch} and $ACS_{Ch}/CODHIII_{Ch}$ in *C. hydrogenoformans* was determined by the supply with CO. Under conditions of excess CO (Fig. 4, which is published as supporting information on the PNAS web site), the ACS_{Ch} was present, and only traces of $ACS_{Ch}/CODHIII_{Ch}$ were apparent. Under conditions of CO limitation (Fig. 4), $ACS_{Ch}/CODHIII_{Ch}$ was formed, and only traces of monomeric ACS_{Ch} were apparent. Free $CODHIII_{Ch}$ was not detectable under any of these conditions.

Catalytic Activities. Both, ACS_{Ch} and $ACS_{Ch}/CODHIII_{Ch}$ catalyzed the exchange of ^{14}C from the carboxyl group of [1-^{14}C]acetyl-CoA with ^{12}C from ^{12}CO (Table 1) at rates that exceeded those reported before of the ACS/CODH from other sources (15, 19). The exchange activity of ACS_{Ch} required the presence of reducing agents such as Ti(III) citrate or dithionite. Maximum activities were obtained with 3 mM Ti(III) citrate. Dithionite (0.2–3 mM) was less effective (<10% of the maximum activity). The exchange activity of ACS_{Ch} was optimal at 70°C and pH 6.0. The K_m was 280 μM acetyl-CoA and V_{max} was 4.4 units·mg^{-1}. The exchange activities of ACS_{Ch} species produced by *C. hydrogenoformans* under different conditions of Cu supply correlated positively with the amounts of Ni present in the enzyme and negatively with the contents of Zn and Cu (Table 1 and Fig. 1*C*). In $ACS_{Ch}/CODHIII_{Ch}$, only Ni and Fe were present in high amounts whereas the Zn and Cu contents were very low and apparently not related to the exchange activity. These data indicate a functional role of Ni in ACS_{Ch} and $ACS_{Ch}/CODHIII_{Ch}$ of *C. hydrogenoformans* and argue against a possible function of Zn and Cu. The sum of Ni, Zn, and Cu in the four preparations of ACS_{Ch} ranged from 1.7 to 1.9 mol per mol (Table 1). This result suggests that Ni in cluster A can be replaced by Zn and/or Cu, yielding an inactive form of the ACS_{Ch}.

ACS_{Ch}, as well as $ACS_{Ch}/CODHIII_{Ch}$, catalyzed the synthesis of acetyl-CoA in the presence of methylcobalamin, CoFeSP from *C. hydrogenoformans*, CO, CoA, and Ti(III) citrate. For ACS_{Ch} and $ACS_{Ch}/CODHIII_{Ch}$ preparations 1 (Table 1), the rate was 0.14 or 0.91 μmol acetyl-CoA formed per min per mg, respectively. ACS_{Ch} showed no CO-oxidation activity whereas this activity in $ACS_{Ch}/CODHIII_{Ch}$ was $\approx$400 μmol CO oxidized per min per mg.

Spectral Properties of ACS_{Ch}. The UV/visible absorption spectrum of ACS_{Ch} in the as-isolated state revealed an FeS-like absorption shoulder extending from 350 to 550 nm that centered around 407 nm (Fig. 1*D*, trace a). This feature was taken as an indication of a $[4Fe\text{-}4S]^{2+}$ cluster. The absorbance of the shoulder did not increase when ACS_{Ch} was exposed to air. Treatment of the as-isolated ACS_{Ch} with dithionite resulted in bleaching of the FeS-like shoulder (Fig. 1*D*, trace b). These data suggest a fully oxidized state of the as-isolated enzyme. The extinction coefficients (ε) of oxidized ACS_{Ch} at 278, 407, or 420 nm were 119.1, 11.8, and 11.2 $mM^{-1}\cdot cm^{-1}$, respectively.

EPR spectra of the as-isolated oxidized ACS_{Ch} recorded in the temperature range of 10–80 K revealed paramagnetic signals at g = 4.3 (not shown) and at g values of 2.03, 2.02, and 1.99 (Fig. 1*E*, trace a), both showing maximum intensity at 10 to 20 K. All signals were very weak and similar to those originating from Fe^{3+} and from an oxidized [3Fe-4S] cluster produced by slight damage of the [4Fe-4S] cluster (33, 34). The spin concentration of the second signal at g = 2.02 (20 K) was 0.02 mol of spin per mol of ACS_{Ch}. As-isolated ACS_{Ch} after reduction with dithionite was EPR-silent in the range 10 to 130 K (Fig. 1*E*, trace b), referring to possible spin interaction between paramagnetic $[4Fe\text{-}4S]^{1+}$ and Ni^{1+}. After treatment of the as-isolated ACS_{Ch} with CO, a strong axial signal with g values of 2.069 and 2.030 appeared (Fig. 1*E*, trace c), which is interpreted as interaction of CO with Ni^{1+} in cluster A. This signal was apparent from 10 to 130 K, with maximum intensity at 20 K. Integration of the signal revealed 0.14 mol of spin per mol of ACS_{Ch}. A similar signal originating from the ACS/CODH of other bacteria has been designated NiFeC signal (18, 35–38).

Overall Structure of ACS_{Ch}. ACS_{Ch} with the highest specific activity (preparation 1 in Table 1) was subjected to crystallization. The polygonal crystals obtained displayed a brown color and had a side length of 0.2 mm. The crystal structure of ACS_{Ch} consists of three domains (Fig. 2*A*). The residues 5–315 belong to the N-terminal domain, the residues 316–500 to the middle domain, and 501–732 to the C-terminal domain. The overall fold is most similar to the "open" conformation of the ACS subunit of $ACS_{Mt}/CODH_{Mt}$ (12), with an rms deviation (rmsd) of 3.5 Å for all Cα-atoms whereas an

BIOCHEMISTRY

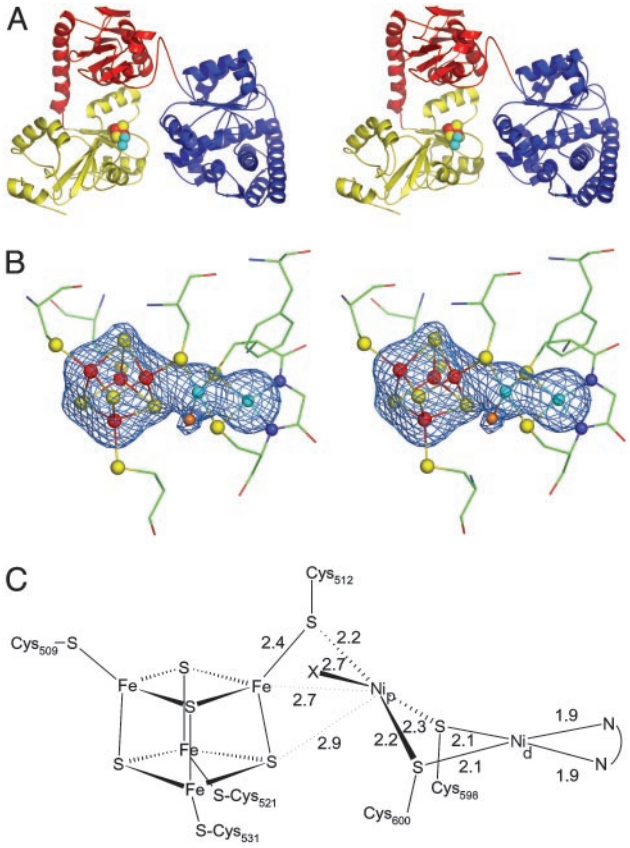

Fig. 2. (*A*) Stereo presentation of the overall fold of the monomeric ACS_{Ch}. The N-terminal domain is depicted in blue, the middle domain is in red, and the C-terminal domain is in yellow. Cluster A is shown as spheres (Ni in cyan, Fe in red, S in yellow). Data in Fig. 2 were obtained with the most active ACS_{Ch} (preparation 1 in Table 1). *A* and *B* were created with PYMOL (39). (*B*) Stereo presentation of the Ni-Ni-[4Fe-4S] cluster A. The 2.2-Å resolution F_{obs}-F_{calc} omit map (blue), contoured at 6.5 σ was calculated after omitting the ''inorganic'' part of cluster A (Ni in cyan, Fe in red, S in yellow, N in blue, water ligand at Ni-p in orange). (*C*) Schematic presentation of cluster A with selected distances. The distance between Ni-d and Ni-p is 3.0 Å. The distance between Ni-p and the nearest Fe ion is only 2.7 Å. X, Proposed water ligand at Ni-p.

rmsd of 8.3 to 8.6 Å is calculated when compared with the "closed" conformation (12) or the conformation reported by Doukov *et al.* (13), respectively.

Structure of Reduced Cluster A. The active site cluster A has been modeled as a Ni-Ni-[4Fe-4S] cluster in which both Ni ions show a square-planar coordination geometry (Fig. 2 *B* and *C*). The six metal ions of cluster A have been identified by their anomalous scattering properties at two wavelengths for Fe (1.733 and 1.7421 Å) and two wavelengths for Ni (1.47 and 1.50 Å) (Table 3). No further anomalous scatterer could be detected by using anomalous difference Fourier calculations at 0.933, 1.05, 1.47, 1.7421, and 1.733 Å (Table 3). The cluster is exposed to an extended cavity between the three domains, but it is coordinated by residues of the C-terminal domain exclusively. The Ni ion, which is distal to the [4Fe-4S] cluster (Ni-d), is coordinated by two backbone N atoms of Gly-599 and Cys-600 and two Cys side chains (Cys-598 and Cys-600). The proximal Ni ion (Ni-p) shows a coordination by three cysteine residues, sharing Cys-512 with the [4Fe-4S] cluster and Cys-598 and Cys-600 with Ni-d. An additional peak in a $F_o - F_c$ map at 7σ contouring in 2.7-Å distance from the Ni-p has been tentatively assigned as a water ligand completing the square-planar ligand geometry around the metal (Fig. 2 *B* and *C*). The occupancy of all atoms of the cluster A, including the proposed water ligand, are comparable and seem to be nearly completely occupied because they show similar B-values, with a maximum deviation of less then 20% from the mean value, and give a featureless $F_o - F_c$ map.

The observed geometry for the cluster A in ACS_{Ch} agrees well with the proposed open conformation of cluster A in ACS_{Mt}/$CODH_{Mt}$ (12) in that it is composed of two Ni ions showing square-planar ligand geometry. Fold and domain arrangement of ACS_{Ch} (Fig. 2*A*) is very similar to that found for the ACS_{Mt} subunit in ACS_{Mt}/$CODH_{Mt}$ from *M. thermoacetica* (12, 13). It can be anticipated that the presence of CODH in this complex does not have a recognizable effect on the overall structure of the ACS. On the other hand, the influence of the metal content of cluster A on the conformation of the domains seems to be profound (12). In the structure of ACS_{Ch}, the occupation of the Ni-p and Ni-d positions was nearly complete (Fig. 2*B*), as judged by their B-values, although metal analysis suggested an occupancy of only 74% (Table 1).

Cluster A is the entity where CO, the methyl group from CoFeSP, and CoA would bind to form acetyl-CoA. The two Ni ions are both accessible for the substrates. There is one empty coordination site at Ni-d and two at Ni-p because ligand X at Ni-p can easily be replaced (Fig. 2*C*). Recent data on the reactivity of compounds modeling the Ni-Ni cluster A (40, 41) suggest a mononuclear mechanism of acetyl formation, in which both the methyl group and CO would bind at the same Ni-ion. The two coordination sites for binding of CO and the methyl group would be available in ACS_{Ch} at Ni-p. The two electrons that are required for the binding of the methyl group at Ni-p could be provided by a disulfide Cys-598–Cys-600 formation, which would function as the previously postulated redox-active D-site (42) or, as recently proposed by Darnault *et al.* (12), by a two electron redox cycle of Ni-p.

Recently three mechanisms of acetyl-CoA synthesis at cluster A have been proposed. The mononuclear mechanism at a Ni-Ni site proposes the binding of CO and the methyl group at Ni-p, generation of an acetyl group and attack of the carbonyl carbon by deprotonated CoA-S^- with the formation of acetyl-CoA (12). The binuclear mechanisms at a Cu-Ni site (13) or at a Ni-Ni site (43) suggest the binding of CO at Cu-p or Ni-p and the binding of the methyl group at Ni-d.

XAS of Oxidized ACS_{Ch}. XAS was performed on the most active ACS_{Ch} (preparation 1 in Table 1) in the as-isolated state, which is oxidized. The Ni-d has a distorted square-planar geometry with two backbone N scatterers and two S scatterers (Fig. 3). The Ni-p is bridged with Ni-d by both of the cystein-sulfur ligands and with one Fe ion of the [4Fe-4S] cluster by Cys-512. The Ni-K edge x-ray absorption near edge structure (XANES) of ACS_{Ch} (Fig. 5, which is published as supporting information on the PNAS web site), a finger print for the metal binding motif, differs from the XANES patterns published for the Ni-d site in ACS_{Mt}/$CODH_{Mt}$ (15, 44). We attribute these differences to the Ni-p contribution. The first shoulder in the rising edge, indicative of square-planar Ni coordination, is lowered. Moreover, an additional peak at 8,347 eV is observed. This finding suggests, for oxidized ACS_{Ch}, nonplanar coordination at the Ni-p binding site. In the absence of any change in oxidation state, this result provides evidence for the structural flexibility of the Ni-p coordination. The Ni content of the ACS_{Ch} XAS sample has been determined to 1.48 Ni ions per protein monomer. Given that Ni-d was suggested (12) and is proven to be nonlabile (17), we assumed full occupancy of this site and 50% occupancy of the Ni-p site. With this model, the Ni coordination was refined to the following: two nitrogen ligands at 1.86 Å and two sulfur ligands at 2.17 Å for Ni-d; and three sulfur ligands at 2.17 Å and one oxygen ligand at 2.32 Å for Ni-p (Fig. 3 and Table 2). The Ni-Ni distance was refined to 2.89 Å, and the distance between Ni-p and the closest Fe ion to 2.71 Å (for details on excluded alternative models, see Fig. 6, which is published as supporting

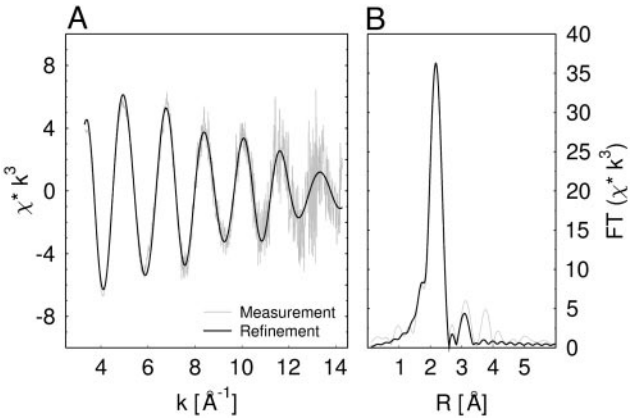

Fig. 3. Ni-K edge EXAFS (*A*) and corresponding Fourier transform (*B*) for ACS_{Ch} (preparation 1 in Table 1) including fit with two nitrogen ligands and two sulfur ligands for Ni-d and three sulfur ligands and one oxygen ligand for Ni-p. All Ni-S distances were assumed to be identical to lower the number of fit parameters. The Ni-metal contributions, refined to 2.9 Å for Ni-Ni and 2.7 Å for Ni-Fe, result in the FT-peak at ≈3 Å due to the first shell phase shift correction applied.

information on the PNAS web site). For both Ni-binding sites, bond valence sum is consistent with a 2+ oxidation state (45). For Ni-d, the value is at the upper and for Ni-p at the lower boundary. Noteworthy, both metal coordinations are consistent with the active site model based on the crystal structure (Fig. 2*C*). This consistency provides independent evidence for the nature of the bridging metal. Moreover, the most probable flexible Ni-p ligand is a water molecule at 2.32-Å distance.

Preliminary sequence data were obtained from The Institute for Genomic Research website at www.tigr.org. Sequencing of *C. hydrogenoformans* was accomplished with support from the United States Department of Energy. We gratefully acknowledge financial support by the Deutsche Forschungsgemeinschaft (SV10/1-1 to V.S. and O.M.), the Fonds der Chemischen Industrie (to O.M.), and a collaborative linkage grant from the North Atlantic Treaty Organization (NATO, LST.CLG.978269).

Table 2. EXAFS curve fitting results for oxidized ACS_{Ch} from CO-grown *C. hydrogenoformans*

Binding site	Shell	N_s	R_s(Å)	σ_s^2(Å²)
Ni-d				
	N	2	1.86 (2)	0.009 (1)
	S	2	2.17 (1)*	0.005 (1)†
	Ni	1	2.89 (1)‡	0.007 (1)§
Ni-p				
	S	3	2.17 (1)*	0.005 (1)†
	O	1	2.32 (4)	0.003 (3)
	Ni	1	2.89 (1)‡	0.007 (1)§
	Fe	1	2.71 (2)	0.007 (1)§

N_s is the number of scatterers per binding site. R_s is the metal-scatterer distance. σ_s^2 is the mean square deviation in R_s (Debye-Waller parameter).

*Individual constrain introduced for the refinement, reducing the number of free parameters. The shift of the energy origin (E = 8,333 eV) was refined to $\Delta E_0 = 0.3$ (10) eV. Bond-valance sum analysis is consistent with the predicted Ni^{2+} oxidation states (2.19 for Ni-d and 1.77 for Ni-p). Numbers in parentheses always give the 2 sigma error of the last digit.

†Individual constrain introduced for the refinement, reducing the number of free parameters. See * for details.

‡Individual constrain introduced for the refinement, reducing the number of free parameters. See * for details.

§Individual constrain introduced for the refinement, reducing the number of free parameters. See * for details.

1. Huber, C. & Wächtershäuser, G. (1997) *Science* **276,** 245–247.
2. Martin, W. & Russel, M. J. (2003) *Philos. Trans. R. Soc. London B. Biol. Sci.* **358,** 59–85.
3. Drake H. L. (1994) in *Acetogenesis*, ed. Drake, H. L. (Chapman & Hall, New York), pp. 3–60.
4. Ferry, J. G. (1995) *Annu. Rev. Microbiol.* **49,** 305–333.
5. Lindahl P. A. (2002) *Biochemistry* **41,** 2097–2105.
6. Ragsdale, S. W. & Kumar, M. (1996) *Chem. Rev.* **96,** 2515–2539.
7. Wood, H. G. (1991) *FASEB J.* **5,** 156–163.
8. Svetlichny, V. A., Sokolova, T. G., Gerhardt, M., Ringpfeil, M., Kostrikina, N. A. & Zavarzin, G. A. (1991) *Syst. Appl. Microbiol.* **14,** 254–260.
9. Svetlitchnyi, V., Peschel, C., Acker, G. & Meyer, O. (2001) *J. Bacteriol.* **183,** 5134–5144.
10. Dobbek, H., Svetlitchnyi, V., Gremer, L., Huber, R. & Meyer, O. (2001) *Science* **293,** 1281–1285.
11. Drennan, C. L., Heo, J., Sintchak, M. D., Schreiter, E. & Ludden, P. W. (2001) *Proc. Natl. Acad. Sci. USA* **98,** 11973–11978.
12. Darnault, C., Volbeda, A., Kim, E. J., Legrand, P., Vernède, X., Lindahl, P. A. & Fontecilla-Camps, J. C. (2003) *Nat. Struct. Biol.* **10,** 271–279.
13. Doukov, T. I., Iverson, T. M., Seravalli, J., Ragsdale, S. W. & Drennan, C. L. (2002) *Science* **298,** 567–572.
14. Shin, W. & Lindahl, P. A. (1992) *Biochemistry* **31,** 12870–12875.
15. Seravalli, J., Gu, W., Tam, A., Strauss, E., Begley, T. P., Cramer, S. P. & Ragsdale, S. W. (2003) *Proc. Natl. Acad. Sci. USA* **100,** 3689–3694.
16. Shin, W. & Lindahl, P. A. (1992) *J. Am. Chem. Soc.* **114,** 9718–9719.
17. Bramlett, M. R., Tan, X. & Lindahl, P. A. (2003) *J. Am. Chem. Soc.* **125,** 9316–9317.
18. Gencic, S. & Grahame, D. A. (2003) *J. Biol. Chem.* **278,** 6101–6110.
19. Raybuck, S. A., Bastian, N. R., Orme-Johnson, W. H. & Walsh, C. T. (1988) *Biochemistry* **27,** 7698–7702.
20. Abbant, D. R. & Ferry, J. G. (1990) *J. Bacteriol.* **172,** 7145–7150.
21. Roberts, J. R., Lu, W.-P. & Ragsdale, S. W. (1992) *J. Bacteriol.* **174,** 4667–4676.
22. Collaborative Computational Project No. 4 (1994) *Acta Crystallogr. D* **50,** 760–763.
23. La Fortelle, E. D., Irwin, J. J. & Bricogne, G. (1997) *Crystallogr. Comput.* **7,** 1–9.
24. Turk, D. (1992) Ph.D. thesis (Technische Universität, Munich, Germany).
25. Brünger, A. T., Adams, P. D., Clore, G. M., DeLano, W. L., Gros, P., Grosse Kunstleve, R. W., Jiang, J. S., Kuszewski, J., Nilges, M., Pannu, N. S., *et al.* (1998) *Acta Crystallogr. D* **54,** 905–921.
26. Pettifer, R. F. & Hermes, C. (1985) *J. Appl. Crystallogr.* **18,** 404–412.
27. Nolting, H. F. & Hermes, C. (1992) EXPROG, EMBL EXAFS Data Analysis and Evaluation Program package (EMBL, Hamburg, Germany).
28. Binsted, N., Strange, R. W. & Hasnain, S. S. (1992) *Biochemistry* **31,** 12117–12125.
29. Beisenherz, G., Bolze, H. J., Bücher, T., Czok, R., Garbade, K. H., Meyer-Arendt, E. & Pfleiderer. G. (1953) *Z. Naturforsch.* **8b,** 555–577.
30. Bradford, M. M. (1976) *Anal. Biochem.* **72,** 248–254.
31. Gremer, L. & Meyer, O. (1996) *Eur. J. Biochem.* **238,** 862–866.
32. Fogo, J. K. & Popowsky, M. (1949) *Anal. Chem.* **21,** 732–734.
33. Albracht, S. P. (1985) *Biochem. Soc. Trans.* **13,** 582–585.
34. Flint, D. H. & Allen, R. M. (1996) *Chem. Rev.* **96,** 2315–2334.
35. Grahame, D. A., Khangulov, S. & DeMoll, E. (1996) *Biochemistry* **35,** 593–600.
36. Lindahl, P. A., Münck, E. & Ragsdale, S. W. (1990) *J. Biol. Chem.* **265,** 3873–3879.
37. Ragsdale, S. W., Wood, H. G. & Antholine, W. E. (1985) *Proc. Natl. Acad. Sci. USA* **82,** 6811–6814.
38. Terlesky, K. C., Nelson, M. J. K. & Ferry, J. G. (1986) *J. Bacteriol.* **168,** 1053–1058.
39. DeLano, W. L. (2003) *The PyMol Molecular Graphics System* (DeLano Scientific LLC, San Carlos, CA).
40. Golden, M. L., Rampersad, M. V., Reibenspies, J. H. & Darensbourg, M. Y. (2003) *Chem. Commun.* **15,** 1824–1825.
41. Linck, R. C., Spahn, C. W., Rauchfuss, T. B. & Wilson. S. R. (2003) *J. Am. Chem. Soc.* **125,** 8700–8701.
42. Barondeau, D. P. & Lindahl P. A. (1997) *J. Am. Chem. Soc.* **119,** 3959–3970.
43. Grahame, D. A. (2003) *Trends Biochem. Sci.* **28,** 221–224.
44. Russel, W. K., Stalhandske, C. M. V., Xia, J., Scott, R. A. & Lindahl, P. A. (1998) *J. Am. Chem. Soc.* **120,** 7502–7510.
45. Liu, W. & Thorp, H. H. (1993) *Inorg. Chem.* **32,** 4102–4105.